

6 NRG with Bosons

Kevin Ingersent

Department of Physics, University of Florida

P.O. Box 188440, Gainesville, FL 32611-8440, USA

Contents

1	Introduction	2
2	NRG with local bosons	3
2.1	The Anderson-Holstein model	3
2.2	NRG solution method	4
2.3	Results	6
3	Bosonic NRG	9
3.1	The spin-boson model	9
3.2	NRG solution method	10
3.3	Results	12
4	Bose-Fermi NRG	16
4.1	The Bose-Fermi Kondo model	16
4.2	NRG solution method	18
4.3	Results	19
5	Closing	23

1 Introduction

The lecture notes in this Autumn School describe many quantum impurity problems of current interest in connection with the physics of strongly correlated electrons, as well as some of the techniques that have been devised to solve these problems. One such technique that has historically been very influential in the understanding of quantum impurity systems is the numerical renormalization group (NRG) method [1–3]. The NRG remains very important for the study of a variety of topical issues (see, e.g., the lecture notes by T. Costi [4]).

The NRG method was developed to provide a robust account of the low-energy properties of Hamiltonians describing the coupling of a local dynamical degree of freedom (a spin or a localized electronic level) to a gapless band of delocalized electrons. These lecture notes focus on extensions of the NRG to treat quantum impurity problems that involve bosonic degrees of freedom. We will consider three classes of problem of increasing complexity:

1. *Local-bosonic* models in which a localized degree of freedom couples not only to band fermions but also to one or more discrete bosonic modes, each representing perhaps an optical phonon mode or a monochromatic light source. Such models arise, for example, in the description of single-molecule devices in which the molecular charge couples to a localized vibration.
2. *Pure-bosonic* models in which the impurity couples to an environment of dispersive bosonic excitations that acts as a source of decoherence on the impurity degrees of freedom. The canonical example of such a problem is the spin-boson model [5,6].
3. *Bose-Fermi* models that couple an impurity both to band fermions and to dispersive bosons, the latter representing, e.g., acoustic phonons or some effective magnetic fluctuations. Such models, which describe not only the key physics of certain nanodevices but also form approximate descriptions of heavy-fermion systems, manifest the phenomenon of critical Kondo destruction.

In each of these cases, it proves possible to preserve the essential strategy of the NRG approach of introducing an artificial separation of energy scales that allows the Hamiltonian to be solved iteratively to provide controlled approximations to physical quantities at a sequence of energy scales extending arbitrarily close to zero. However, the presence of bosons imposes greater computational challenges since the Fock space of the problem is of infinite dimension even in the atomic limit where one neglects the energy dispersion of the environmental excitations. As a result, state truncation plays a greater role than in conventional NRG calculations and it proves to be very important to make an appropriate choice of bosonic basis states.

The sections that follow treat in turn the three classes of problem identified above. For each class, a representative model is introduced and physically motivated. The extension of the conventional (pure-fermionic) NRG method to solve this problem is described and illustrative results are presented.

2 NRG with local bosons

2.1 The Anderson-Holstein model

The Anderson-Holstein model has been studied since the 1970s in connection with mixed valence [7–10], negative- U centers in superconductors [11–13], and most recently, single-molecule devices [14–16]. Its Hamiltonian is $H_{\text{AH}} = H_{\text{A}} + H_{\text{LB}}$, where [17]

$$H_{\text{A}} = \varepsilon_d n_d + U n_{d\uparrow} n_{d\downarrow} + \sum_{\mathbf{k}, \sigma} \varepsilon_{\mathbf{k}} c_{\mathbf{k}\sigma}^\dagger c_{\mathbf{k}\sigma} + \frac{1}{\sqrt{N_k}} \sum_{\mathbf{k}, \sigma} V_{\mathbf{k}} (d_\sigma^\dagger c_{\mathbf{k}\sigma} + \text{H.c.}) \quad (1)$$

describes the standard Anderson impurity model [18] in which d_σ annihilates an electron of spin z component $\sigma = \pm\frac{1}{2}$ (or $\sigma = \uparrow, \downarrow$) and energy ε_d in the impurity level, $n_d = n_{d\uparrow} + n_{d\downarrow}$ (with $n_{d\sigma} = d_\sigma^\dagger d_\sigma$) is the total impurity occupancy, and $U > 0$ is the Coulomb repulsion between two electrons in the impurity level. $V_{\mathbf{k}}$ is the hybridization matrix element between the impurity and a conduction-band state of energy $\varepsilon_{\mathbf{k}}$ annihilated by fermionic operator $c_{\mathbf{k}\sigma}$, while N_k is the number of unit cells in the host metal and, hence, the number of inequivalent \mathbf{k} values. The local boson Hamiltonian term

$$H_{\text{LB}} = \omega_0 b^\dagger b + \lambda(n_d - 1)(b + b^\dagger). \quad (2)$$

describes the linear coupling of the impurity occupancy to the displacement of a local bosonic mode of frequency ω_0 . Without loss of generality, we can take the electron-boson coupling λ to be real and non-negative.

The conduction-band dispersion $\varepsilon_{\mathbf{k}}$ and the hybridization $V_{\mathbf{k}}$ affect the impurity degrees of freedom only through the hybridization function $\Delta(\varepsilon) \equiv (\pi/N_k) \sum_{\mathbf{k}} V_{\mathbf{k}}^2 \delta(\varepsilon - \varepsilon_{\mathbf{k}})$. To focus on universal physics of the model, we assume a featureless form

$$\Delta(\varepsilon) = \Delta \Theta(D - |\varepsilon|), \quad (3)$$

where D is the half-bandwidth and $\Theta(x)$ is the Heaviside step function.

In the case $\Delta = 0$ of an isolated impurity, the impurity occupancy n_d is fixed, and it is possible to eliminate the electron-boson coupling (the second term in H_{LB}) from H_{AH} via the substitution $b \rightarrow \tilde{b} = b + (\lambda/\omega_0)(n_d - 1)$, which maps the Anderson-Holstein model to an Anderson model plus a free boson mode: $H_{\text{AH}} = \tilde{H}_{\text{A}} + \omega_0 \tilde{b}^\dagger \tilde{b}$, where \tilde{H}_{A} is identical to H_{A} apart from the replacement of the level energy ε_d and the Coulomb repulsion U by

$$\tilde{\varepsilon}_d = \varepsilon_d + \omega_p, \quad \tilde{U} = U - 2\omega_p, \quad \text{where } \omega_p = \lambda^2/\omega_0 \quad (4)$$

is called the *polaron energy* in the context of electron-phonon coupling. The physical content of Eq. (4) is that H_{LB} describes a quantum harmonic oscillator displaced by a constant force proportional to $\lambda(n_d - 1)$. For $n_d \neq 1$, the ground state of the displaced oscillator is a coherent state of energy $-\omega_p$ (relative to the undisplaced ground state for $n_d = 1$) in which the boson occupation $n_b = b^\dagger b$ follows a Poisson distribution $P(n_b) = \exp(-\bar{n}_b) (\bar{n}_b)^{n_b}/n_b!$ with mean $\bar{n}_b = (\lambda/\omega_0)^2$. This lowering of the ground-state energy can be captured by the effective

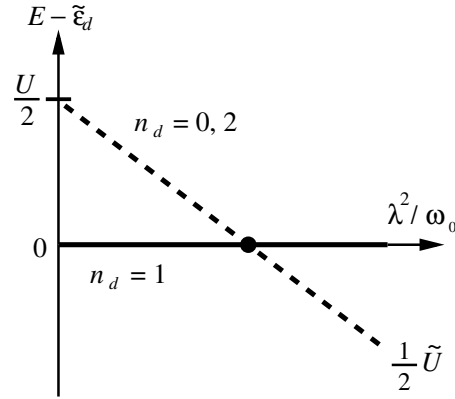


Fig. 1: Evolution with polaron energy $\omega_p = \lambda^2/\omega_0$ of $E - \tilde{\varepsilon}_d$, where E is the lowest energy in each n_d sector of the Anderson-Holstein model for $\varepsilon_d = -\frac{1}{2}U$ (particle-hole symmetry) and $\Delta = 0$ (no hybridization), while $\tilde{\varepsilon}_d$ is the energy of the lowest $n_d = 1$ spin doublet. The gap $\frac{1}{2}\tilde{U}$ to the lowest energy in the sectors $n_d = 0, 2$ vanishes at $\omega_p = \frac{1}{2}U$. For $\omega_p > \frac{1}{2}U$, the system has a charge-doublet ground state. Adapted from [19].

renormalization of Anderson model parameters according to Eq. (4). As shown in Fig. 1, for $\omega_p > U/2$ the effective Coulomb interaction on the impurity site becomes negative, and for the special case $\varepsilon_d = -\frac{1}{2}U$ of exact particle-hole symmetry the ground state passes from a spin doublet to a charge doublet.

When the impurity-band hybridization is switched on, the effect of the electron-boson coupling remains fully captured by Eq. (4) only if ω_0 is so large that the boson distribution adjusts essentially instantaneously each time that n_d changes. More generally, though, each hybridization event causes the emission and absorption of a cloud of bosons that relaxes with a characteristic time scale ω_0^{-1} toward the distribution favored by the new impurity occupancy [9]. If ω_0^{-1} is comparable with or longer than the characteristic time scale for impurity-band tunneling, the relaxation is incomplete by the time the next hybridization event unleashes another boson cloud. This creates inertia in the system that manifests itself as a reduction in the effective hybridization width Δ . The resulting interplay of impurity charge fluctuations, strong electron-electron correlations, and electron-boson coupling can be treated analytically only in certain limiting cases [9, 14]. In order to obtain a nonperturbative account of the physics over the full parameter space, an NRG treatment of the Anderson-Holstein model is very desirable.

2.2 NRG solution method

As described in greater detail in the other lecture notes [4], there are three essential steps in the NRG treatment of a pure-fermionic problem such as that described by H_A :

1. Division of the band energies $-D \leq \varepsilon < D$ into logarithmic bins spanning $DA^{-(m+1)} \leq \pm\varepsilon < DA^{-m}$ for $A > 1$ and $m = 0, 1, 2, \dots$. Within each bin, the continuum of band states is replaced by a discrete state, namely, the linear combination [weighted according to the hybridization function $\Delta(\varepsilon)$] that interacts with the impurity. The states from adjacent bins have average energies that differ by a factor of A .

2. The Lanczos method [20] is applied to perform a canonical transformation on the discrete bin states, mapping the conduction band onto a semi-infinite tight-binding chain that couples to the impurity only at the end site $n = 0$:

$$H_{\text{band}} = \sum_{\mathbf{k}, \sigma} \varepsilon_{\mathbf{k}} c_{\mathbf{k}\sigma}^\dagger c_{\mathbf{k}\sigma} \simeq D \sum_{n=0}^{\infty} \sum_{\sigma} t_{n+1} (f_{n\sigma}^\dagger f_{n+1, \sigma} + \text{H.c.}), \quad (5)$$

where the chain-site creation and annihilation operators obey $\{f_{n\sigma}, f_{n'\sigma'}^\dagger\} = \delta_{n,n'} \delta_{\sigma,\sigma'}$ and the dimensionless hopping coefficients drop off as $t_n \simeq \Lambda^{-n/2}$ due to the separation of energy scales in the discretized band.

3. Iterative diagonalization of scaled Hamiltonians H_N on chains truncated at length $N + 1$, starting with (for the Anderson impurity model)

$$H_0 = \varepsilon_d n_d + U n_{d\uparrow} n_{d\downarrow} + \sqrt{\frac{2\Delta D}{\pi}} \sum_{\sigma} (d_{\sigma}^\dagger f_{0\sigma} + \text{H.c.}). \quad (6)$$

The basis of H_N has dimension $d_N = 4^{N+2}$, requiring storage $\propto d_N^2$ and a solution time $\propto d_N^3$. It therefore becomes necessary after only a few iterations to truncate the basis. In most cases, one retains at the end of iteration N just the N_s states of lowest energy (with N_s typically lying in the range 100 to 1000) so that the basis of H_{N+1} has a reduced dimension $d_{N+1} = 4N_s$. Under this procedure, the low-lying many-body eigenstates of H_N (a) describe the essential physics on energy and temperature scales of order $D\Lambda^{-N/2}$, and (b) provide a good starting point for finding the low-lying eigenstates of $H_{N+1} = \Lambda^{1/2}(H_N - E_N^{(0)}) + D t_{N+1} \Lambda^{(N+1)/2} \sum_{\sigma} (f_{N\sigma}^\dagger f_{N+1, \sigma} + \text{H.c.})$, where $E_N^{(0)}$ is the ground-state energy of iteration N . The rescaling of H_{N+1} by a multiplicative factor of $\sqrt{\Lambda}$ relative to H_N facilitates the identification of renormalization-group fixed-points characterized by self-similar many-body spectra [1, 2].

Going from H_A to H_{AH} does not require any modification of steps 1 and 2 above. At step 3, however, H_{LB} in Eq. (2) must be added into H_0 in Eq. (6). For the Anderson model, the Fock space of iteration 0 has dimension 4 (for the impurity) \times 4 (for chain site 0) = 16, which makes numerical diagonalization of H_0 a trivial matter. The inclusion of bosonic degrees of freedom that are not limited by the Pauli exclusion principle immediately has the effect of raising the Fock-space dimension to infinity. Since diagonalization of infinite matrices is computationally infeasible, one is forced to introduce the additional approximation (relative to the pure-fermionic NRG) of truncating the basis of H_0 .

The low-lying many-body states of H_0 should be superpositions of configurations in which n_d takes each of its possible values. We therefore expect to have to be able to capture both (a) configurations with low values of n_b that are energetically favorable for $n_d = 1$ and (b) configurations with boson distributions close to the coherent states favored for $n_d = 0$ and 2. Given the rapid fall-off of the coherent-state boson occupation distribution $P(n_b) = \exp(-\bar{n}_b) (\bar{n}_b)^{n_b} / n_b!$ for $n_b \gg \bar{n}_b = (\lambda/\omega_0)^2$, one can hope to work with a bosonic basis consisting of all occupation number eigenstates with $0 \leq n_b < N_b$. Hewson and Meyer [9] established a criterion

$N_b \geq 4\bar{n}_b$. However, in view of the standard deviation $\sigma_b = \sqrt{\bar{n}_b}$ of the Poisson distribution it seems probable that for large \bar{n}_b it would be more efficient to select $N_b = \bar{n}_b + c\sigma_b$ with c being a fixed number of order 5. Better still might be a basis that directly includes the ground state and low-lying excitations of the displaced oscillators, i.e., eigenstates of well-defined and small $\tilde{b}^\dagger\tilde{b}$. However, exploration of such an option has been rendered unnecessary by the success of the simpler basis $0 \leq n_b < N_b$. This basis increases the CPU time for iteration 0, which is proportional to $(16N_b)^3$, but leaves unaffected the generally much greater CPU time $\propto (4N_s)^3$ for high iteration numbers.

2.3 Results

We begin by considering results for the symmetric Anderson-Holstein model ($\varepsilon_d = -\frac{1}{2}U$) where the impurity-boson subsystem has a level-crossing from a magnetic ground state (for $\lambda < \lambda_c$) to a non-magnetic charge-doublet ground state (for $\lambda > \lambda_c$). Figure 2 plots three temperature scales extracted from thermodynamic properties calculated using the NRG:

- $T_s = 0.103/\chi_s(T = 0)$, where $\chi_s(T)$ is the impurity contribution to the system's static spin susceptibility, i.e., the difference between the spin susceptibility $(\langle S_z^2 \rangle - \langle S_z \rangle^2)/T$ (S_z being the z component of the system's total spin) with and without the impurity. The impurity spin degree of freedom is quenched for $T \lesssim T_s$, and in the Kondo regime $0 < \Delta \ll -\varepsilon_d, U + \varepsilon_d$ of the Anderson model [2], T_s coincides with the Kondo temperature.
- $T_c = 0.412/\chi_c(T = 0)$, where $\chi_c(T)$ is the impurity contribution to the static charge susceptibility $(\langle Q^2 \rangle - \langle Q \rangle^2)/T$ with Q being the total electron number measured from half-filling. The impurity charge is quenched for $T \lesssim T_c$, and in the regime $0 < \Delta \ll \varepsilon_d, -(U + \varepsilon_d)$ of the negative- U Anderson model, T_c is the Kondo temperature characterizing a many-body screening of the impurity charge directly analogous to the standard (spin) Kondo effect [21, 22]. The different coefficients in the definitions of T_s and T_c reflect the values $\chi_s = 1/(4T)$ for a free spin doublet and $\chi_c = 1/T$ for a free charge doublet.
- T_K defined via the impurity contribution to the entropy via the condition $S_{\text{imp}}(T_K) = 0.383$. T_K can be regarded as the crossover temperature for the suppression of all impurity degrees of freedom and coincides with the relevant Kondo temperature in the spin-Kondo and charge-Kondo regimes of the Anderson model.

Figure 2 provides evidence for a smooth crossover with increasing electron-boson coupling from a spin-Kondo effect to a charge-Kondo effect. As ω_p increases from zero, T_s rises rapidly as the impurity loses its local-moment character and the system crosses from the strongly correlated spin-Kondo regime to the weakly correlated mixed-valence regime as \tilde{U} falls toward zero from its initial value of U . At the same time, T_c decreases from very large values at $\omega_p = 0$ and becomes exponentially small in the charge-Kondo regime $\omega_p \gg \frac{1}{2}U = 0.1D$ where \tilde{U} is large and negative. Meanwhile, T_K evolves from following T_s deep in the spin-Kondo regime

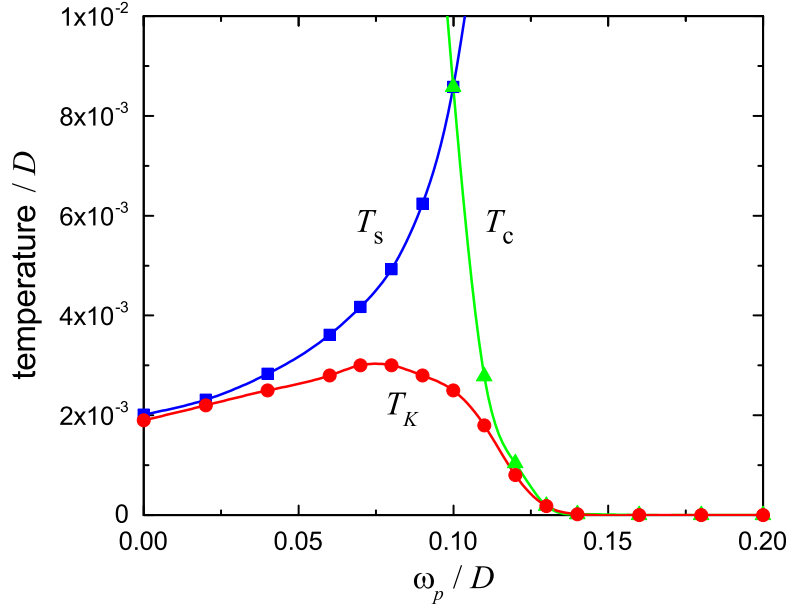


Fig. 2: Variation with the polaron energy $\omega_p = \lambda^2/\omega_0$ of three energy scales for the particle-hole-symmetric Anderson-Holstein model with $U = -2\varepsilon_d = 0.2D$, $\Delta = 0.032D$, and $\omega_0 = 0.05D$: the spin-screening temperature T_s , the charge-screening temperature T_c , and the Kondo temperature T_K extracted from the impurity entropy via the condition $S_{\text{imp}}(T_K) = 0.383$. NRG results obtained for $\Lambda = 2.5$ with bosonic cutoff $N_b = 16$, retaining up to 2000 many-body states (spin multiplets) after each iteration.

to tracking T_c deep in the charge-Kondo regime. In the intermediate region near $\omega_p = \frac{1}{2}U$, T_K is much smaller than either T_s or T_c , pointing to a many-body Kondo effect of mixed spin and charge character.

The plot of T_K vs. ω_p in Fig. 2 is clearly asymmetric about its peak near $\omega_p = \frac{1}{2}U$. This asymmetry can be seen more clearly in Fig. 3, which plots an effective Kondo energy scale (in this case, extracted from the impurity spectral function) vs λ/ω_0 . For $\omega_p \ll \frac{1}{2}U$ (which for the parameters used in Fig. 3 means $\lambda/\omega_0 \ll 1$), $\Gamma(\lambda)$ is captured by a perturbative mapping [14] onto the Kondo model that incorporates effects beyond the replacement of ε_d and U by $\tilde{\varepsilon}_d$ and \tilde{U} given in Eq. (4). Upon increase of ω_p beyond $\frac{1}{2}U$, Γ drops off extremely fast (note the logarithmic vertical axis in Fig. 3) in a manner that is described quite well by a perturbative mapping to an *anisotropic* charge-Kondo model in which the rate J_\perp of charge-flip impurity-band scattering ($n_d = 0 \rightarrow 2$ and its time reverse, both via an $n_d = 1$ virtual state) is smaller than the rate J_\parallel of charge-conserving scattering ($n_d = 0 \rightarrow 0$ and $n_d = 2 \rightarrow 2$, also both via $n_d = 1$) by a factor $J_\perp/J_\parallel \simeq \exp(-2\lambda^2/\omega_0^2)$. This confirms the extremely strong suppression of real (non-virtual) charge fluctuations caused by the small overlap between the bosonic ground states in each sector of different n_d . In the vicinity of $\omega_p = \frac{1}{2}U$, neither perturbative approach is satisfactory, and one must rely on the full machinery of the NRG to provide reliable results.

Finally, in this section we consider the effect of moving away from particle-hole symmetry of the impurity level. For $\varepsilon_d \neq -\frac{1}{2}U$, the $n_d = 2$ curve in Fig. 1 is raised above the solid line (which now represents just $n_d = 0$) by an amount $U + 2\varepsilon_d$ independent of the electron-boson

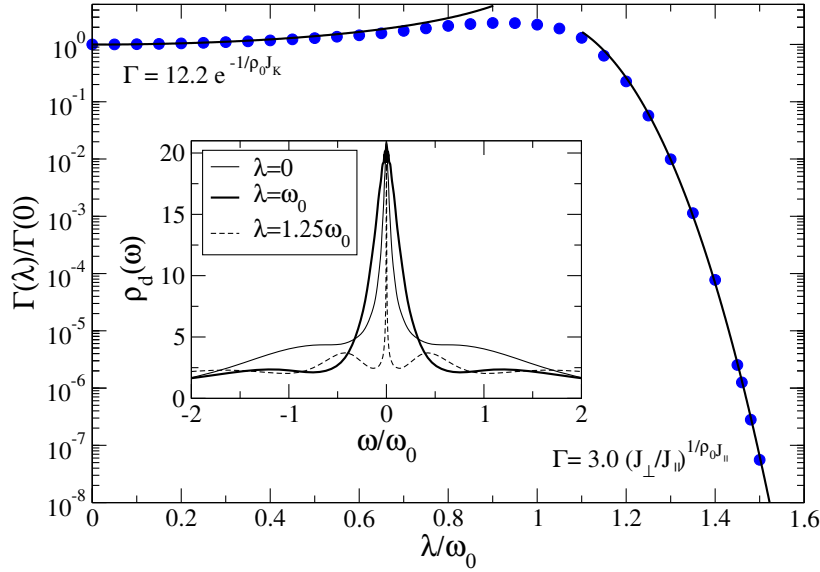


Fig. 3: Variation with λ/ω_0 of an effective Kondo energy scale Γ for the particle-hole-symmetric Anderson-Holstein model with $U = -2\varepsilon_d = 0.1D$, $\Delta = 0.012D$, and $\omega_0 = 0.05D$. Γ is the width of the Abrikosov-Suhl resonance in the impurity spectral function $\rho_d(\omega)$ (see inset). Circles represent NRG data while solid lines are the results of analytical approximations. Reprinted figure with permission from P.S. Cornaglia, H. Ness, and D.R. Grempel, *Phys. Rev. Lett.* **93**, 147201 (2004). Copyright 2004 by the American Physical Society.

coupling. This shift splits the impurity charge doublet in a manner analogous to the action of a magnetic field on the $n_d = 1$ spin doublet, and in the charge-Kondo regime an impurity asymmetry $|U + 2\varepsilon_d| \gg T_c$ suppresses the Kondo effect.

Fig. 4 shows the linear conductance G through a nanodevice in which a single molecule bridges the gap between two electrical leads. The transport is assumed to be dominated by a single, strongly correlated molecular level of energy ε_d (which may be tuned via a voltage applied to an electrical gate) and whose charge couples to a local vibrational mode in a manner described by the Anderson-Holstein model. In such a device [14],

$$G = \frac{2e^2}{h} \pi \Delta \int_{-\infty}^{\infty} d\omega \left(-\frac{\partial f}{\partial \omega} \right) \rho_d(\omega), \quad (7)$$

where $\rho_d(\omega) = -\pi^{-1} \text{Im} G_{dd}(\omega)$, with G_{dd} being the retarded Green's function for the active impurity level. For $\lambda = 0$, Fig. 4a, the conductance at a comparatively high temperature $T = \Delta$ exhibits the phenomenon of Coulomb blockade, where the strong interactions in the molecular level suppress conductance via sequential tunneling of electrons from the source electrode into the molecule and then off into the drain electrode, except near the point $\varepsilon_d = 0$ (or $\varepsilon_d = -U$) of degeneracy between states of occupancy $n_d = 0$ and 1 (or $n_d = 1$ and 2). At $T = 0$, however, G is nonzero due to the formation of the collective Kondo ground state that allows electrons to pass from one lead to another without incurring an energy penalty U . For $\lambda = 0.4\omega_0$, Fig. 4b, the physics is similar, except the spacing between the Coulomb blockade peaks has diminished from U to roughly \tilde{U} . For still larger values of λ such that $\tilde{U} < 0$, Fig. 4d, the high-temperature

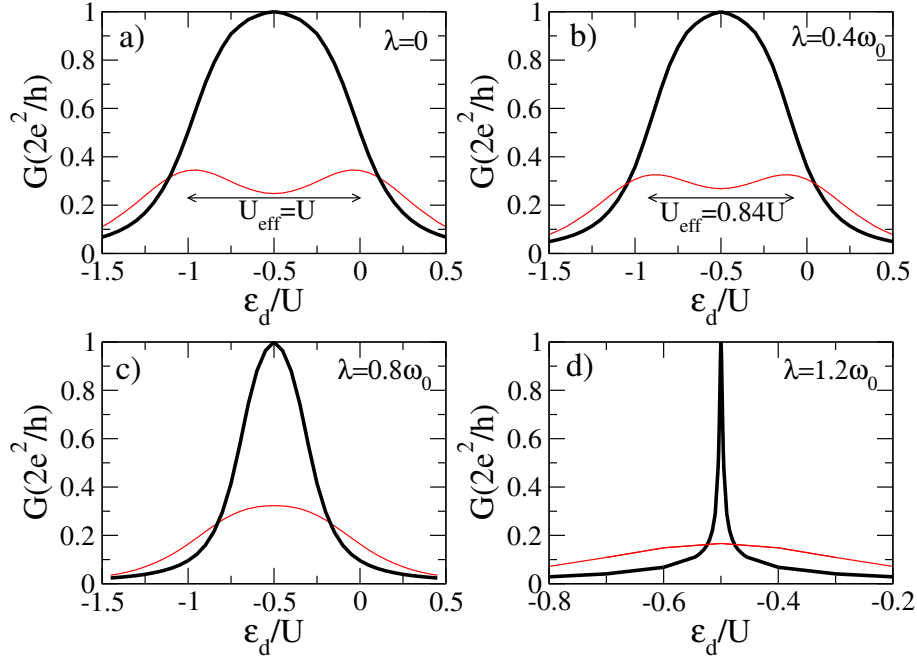


Fig. 4: Linear conductance G vs. level energy ε_d for a single-molecule device described by the Anderson-Holstein model with $U = 0.1$, $\Delta = 0.016$, $\omega = 0.05$, and different values of λ . Thin (thick) lines show NRG results for temperature $T = \Delta$ ($T = 0$). Reprinted figure with permission from P.S. Cornaglia, H. Ness, and D.R. Grempel, *Phys. Rev. Lett.* **93**, 147201 (2004). Copyright 2004 by the American Physical Society.

conductance is suppressed for all values of ε_d because there is no point of degeneracy between ground states differing by 1 in their charge. A charge-Kondo peak remains centered at particle-hole symmetry, but it is very narrow since the many-body Kondo state is essentially destroyed once the charge-doublet splitting $|U + 2\varepsilon_d|$ exceeds the Kondo scale.

3 Bosonic NRG

3.1 The spin-boson model

The spin-boson model for a dissipative two-state system has been heavily studied in many contexts [5, 6], including chemical reactions, motion of defects in solids, biological molecules, and quantum information. Its Hamiltonian can be written [17] $H_{\text{SB}} = -\Delta S_x - h S_z + H_{\text{B}}$, where

$$H_{\text{B}} = \sum_q \omega_q a_q^\dagger a_q + \frac{S_z}{\sqrt{N_q}} \sum_q \lambda_q (a_q + a_q^\dagger). \quad (8)$$

Here, S_x and S_z are the x and z components of the spin (or pseudospin) of a two-state impurity system and a_q annihilates a boson of energy ω_q [17]. Δ is the matrix element for tunneling between states $|\uparrow\rangle$ ($S_z = \frac{1}{2}$) and $|\downarrow\rangle$ ($S_z = -\frac{1}{2}$), h is a (pseudo)magnetic field that couples to the z component of the local spin, N_q is the number of boson modes, and λ_q is a linear coupling between the displacement of mode q and the local spin z . The values of ω_q and λ_q

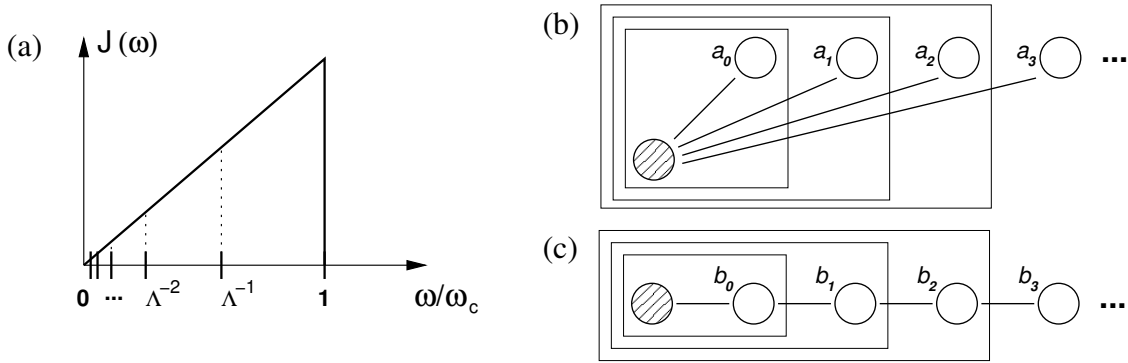


Fig. 5: NRG treatment of a bosonic bath: (a) The bath spectral function is divided into logarithmic bins. (b) The impurity (shaded circle) interacts with one representative state (open circle) from each logarithmic bin $m = 0, 1, 2, \dots$ in a “star” Hamiltonian form. (c) The Lanczos procedure maps the Hamiltonian to a “chain” form where the impurity interacts with just the end site $n = 0$. In (b) and (c), boxes from innermost to outermost enclose the degrees of freedom treated at NRG iterations $N = 0, 1, \text{ and } 2$. Reprinted figures with permission from R. Bulla, H.-J. Lee, N.H. Tong, and M. Vojta, *Phys. Rev. B* **71**, 045122 (2005). Copyright 2005 by the American Physical Society.

enter the problem only in a single combination, the bosonic bath spectral function $J(\omega) = (\pi/N_q) \sum_q \lambda_q^2 \delta(\omega - \omega_q)$, which in the thermodynamic limit $N_q \rightarrow \infty$ generally becomes a smooth function. The most important feature of $J(\omega)$ is its asymptotic low-frequency behavior, so it is conventional to study power-law spectra

$$J(\omega) = 2\pi\alpha\omega_c(\omega/\omega_c)^s\Theta(\omega)\Theta(\omega_c - \omega), \quad (9)$$

where α is a dimensionless dissipation strength, ω_c is a high-frequency cut-off and the bath exponent must satisfy $s > -1$ to allow normalization. The most subtle physics occurs for bath exponents $0 < s \leq 1$, which admit two distinct phases distinguished by an order parameter $\phi = \lim_{h \rightarrow 0^+} \langle S_z \rangle$. In the *delocalized* phase ($\alpha < \alpha_c$), the effective value of α renormalizes to zero, leading to a singlet ground state and $\phi = 0$. In the *localized* phase ($\alpha > \alpha_c$), Δ renormalizes to zero, asymptotically confining the impurity to one or other of its two states and yielding (at least for bias field $h = 0$) a doublet ground state with $\phi > 0$. In the heavily studied case $s = 1$ of an ohmic bath, the quantum phase transition occurs at $\alpha_c = 1 + O(\Delta/\omega_c)$ and is known to be Kosterlitz-Thouless-like [5], involving a jump in the order parameter but a correlation length that diverges on approach from the delocalized side. For sub-ohmic bath exponents $0 < s < 1$, the transition takes place at $\alpha_c \propto (\Delta/\omega_c)^{1-s}$ and is believed to be continuous [23].

3.2 NRG solution method

For $s = 1$, the spin-boson model may be mapped to the anisotropic Kondo model [24] and thus can be treated using the conventional NRG method [25]. However, no such mapping exists for general values of s . The direct NRG treatment of the spin-boson model was pioneered by Bulla

et al. [26, 27]. One can follow the same three essential steps found in the conventional NRG (see Sec. 2.2). After logarithmic binning of the bath, Fig. 5a, the impurity interacts with one representative state from each bin, destroyed by an operator a_m , see Fig. 5b, allowing the bath part of H_{SB} to be written

$$H_{\text{bath}} = \sum_q \omega_q a_q^\dagger a_q \simeq \omega_c \sum_{m=0}^{\infty} \xi_m a_m^\dagger a_m, \quad (10)$$

where the operators a_m obey canonical bosonic commutation relations $[a_m, a_{m'}^\dagger] = \delta_{m,m'}$ and have dimensionless oscillator energies

$$\xi_m = \int_{\omega_c \Lambda^{-(m+1)}}^{\omega_c \Lambda^{-m}} \omega J(\omega) d\omega \Big/ \omega_c \int_{\omega_c \Lambda^{-(m+1)}}^{\omega_c \Lambda^{-m}} J(\omega) d\omega = \frac{1+s}{2+s} \frac{1 - \Lambda^{-(2+s)}}{1 - \Lambda^{-(1+s)}} \Lambda^{-m}. \quad (11)$$

Application of the Lanczos procedure converts this “star form” of the bath Hamiltonian to a tight-binding “chain form”, see Fig. 5c

$$H_{\text{bath}} \simeq \omega_c \sum_{n=0}^{\infty} \left[\varepsilon_n b_n^\dagger b_n + \tau_{n+1} (b_n^\dagger b_{n+1} + \text{H.c.}) \right], \quad (12)$$

where $[b_n, b_{n'}^\dagger] = \delta_{n,n'}$. The fact that $J(\omega) = 0$ for $\omega < 0$ causes the dimensionless on-site energies ε_n and hopping coefficients τ_n to take values of order Λ^{-n} , dropping off with increasing n at a rate twice as fast as the parameters $t_n \approx \Lambda^{-n/2}$ in the fermionic NRG.

Bulla *et al.* [26, 27] constructed two different iterative NRG procedures for the spin-boson model, one based on the star form of H_{bath} and the other based on the chain form:

1. The star-based NRG procedure is illustrated schematically in Fig. 5(b). It starts from an initial Hamiltonian

$$H_0 = -\Delta S_x - h S_z + \omega_c \left[\xi_0 a_0^\dagger a_0 + \sqrt{\frac{2\alpha}{1+s}} S_z \gamma_0 (a_0 + a_0^\dagger) \right] \quad (13)$$

that includes only the bosonic operator a_0 representing the highest-energy logarithmic bin and proceeds to incorporate one more bin at each subsequent iteration according to

$$H_{N+1} = \Lambda (H_N - E_N^{(0)}) + \Lambda^{N+1} \omega_c \left[\xi_{N+1} a_{N+1}^\dagger a_{N+1} + \sqrt{\frac{2\alpha}{1+s}} S_z \gamma_{N+1} (a_{N+1} + a_{N+1}^\dagger) \right]. \quad (14)$$

In Eqs. (13) and (14), γ_m is a positive normalization constant satisfying

$$\gamma_m^2 = \frac{1+s}{2\pi\alpha} \int_{\omega_c \Lambda^{-(m+1)}}^{\omega_c \Lambda^{-m}} d\omega J(\omega) = [1 - \Lambda^{-(1+s)}] \Lambda^{-(1+s)m}. \quad (15)$$

Each operator a_m couples only to the impurity, allowing the bosonic basis to be optimized (at least for $\Delta = 0$, where the impurity becomes static) by transforming to displaced oscillators with annihilation operators $\tilde{a}_m = a_m \pm \theta_m$, where $\theta_m = \sqrt{\alpha/2(1+s)} \gamma_m / \xi_m \sim$

$\Lambda^{(1-s)m/2}$. Since the ground state of the displaced oscillator corresponds to $\langle b_m^\dagger b_m \rangle = \theta_m^2 \sim \Lambda^{(1-s)m}$, a basis of eigenstates of $b_m^\dagger b_m$ restricted to n_{b_m} less than some finite N_b will prove inadequate for capturing the low-energy behavior for any sub-ohmic case $s < 1$. It will be shown in Sec. 3.3 that the same conclusion holds throughout the localized phase of the full sub-ohmic spin-boson model with $\Delta > 0$, but that success can be achieved using a suitably chosen basis of N_b displaced oscillator states optimized for the value of θ_m .

2. The chain-based NRG procedure, which is illustrated schematically in Fig. 5c, starts from an initial Hamiltonian

$$H_0 = -\Delta S_x - h S_z + \omega_c \left[\varepsilon_0 b_0^\dagger b_0 + \sqrt{\frac{2\alpha}{1+s}} S_z (b_0 + b_0^\dagger) \right] \quad (16)$$

where $b_0 = \sum_{m=0}^{\infty} \gamma_m a_m$ and $\varepsilon_0 = (1+s)/(2+s)$. The iteration relation is

$$H_{N+1} = \Lambda(H_N - E_N^{(0)}) + \Lambda^{N+1} \left[\varepsilon_{N+1} b_{N+1}^\dagger b_{N+1} + \tau_{N+1} (b_N^\dagger b_{N+1} + \text{H.c.}) \right], \quad (17)$$

where the Λ^{-N} decay of the tight-binding coefficients ε_N and τ_N dictates a rescaling of H_{N+1} by a factor of Λ (instead of $\sqrt{\Lambda}$ as in the fermionic NRG).

For $\Delta = h = 0$, H_0 describes a displaced harmonic oscillator having a ground state in which the occupation number $n_{b_0} \equiv \langle b_0^\dagger b_0 \rangle$ has a mean value $\bar{n}_{b_0} = \alpha/[2(1+s)\varepsilon_0^2] = \alpha(2+s)^2/[2(1+s)^3]$. The α values of greatest interest are those near α_c , of order 1 or smaller. Therefore, just as in the NRG treatment of the Anderson-Holstein model [Sec. 2.2], it should be satisfactory to use a basis of bosonic number eigenstates with $n_{b_0} < N_b$, where $N_b \geq 4\bar{n}_{b_0}$. However, what is unclear *a priori* is whether a bosonic truncation $n_{b,N+1} < N_b$ will prove satisfactory during subsequent iterations of Eq. (17).

The star and the chain NRG formulations will be seen in Sec. 3.3 to have different strengths and weaknesses. In both cases, a key challenge is to find a bosonic basis size N_b for each site sufficiently large that the physical results are a good approximation to those for $N_b \rightarrow \infty$ while keeping the computational time ($\propto B_b^3$) within acceptable bounds.

3.3 Results

3.3.1 Truncation effects in the chain and star formulations

Bulla *et al.* systematically investigated the effects of basis truncation in the star and chain versions of the bosonic NRG [27]. Figure 6a shows results for the chain NRG, which was the first of the two to be implemented [26]. Throughout the delocalized phase and on the phase boundary, $\langle b_{N+1}^\dagger b_{N+1} \rangle$ for a large fixed N (the figure illustrates $N = 20$ for $s = 0.6$ and $\Delta = 0.01\omega_c$) converges rapidly with increasing N_b to a value much smaller than N_b . For $\alpha > \alpha_c$, however, $\langle b_{N+1}^\dagger b_{N+1} \rangle$ continues to grow with N_b . Although the average boson occupancy saturates for sufficiently large values of N_b , the size of the basis required to eliminate truncation effects

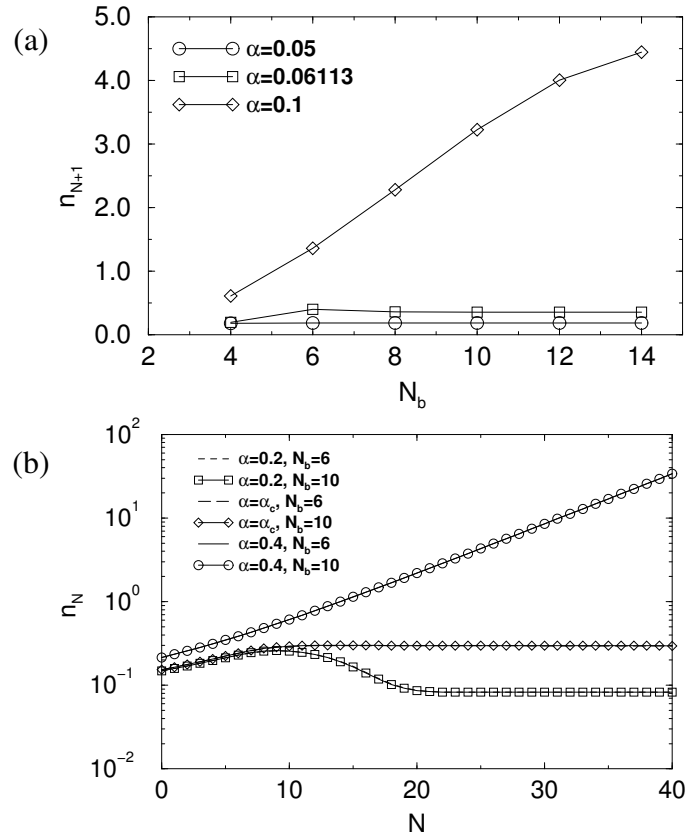


Fig. 6: Effects of bosonic basis truncation in the NRG treatment of the sub-ohmic spin-boson model: (a) Average occupancy of bosonic chain site 21 vs. bosonic truncation parameter N_b within the chain NRG. Data for $s = 0.6$, $\Delta = 0.01\omega_c$, $\Lambda = 2$, and for α below, at, and above $\alpha_c = 0.06113$. (b) Average occupancy $n_N = \langle b_N^\dagger b_N \rangle$ vs. bosonic bin index N within the star NRG. Data for $s = 0.8$, $\Delta = 0.01\omega_c$, and $\Lambda = 2$, obtained for α below, at, and above α_c using an optimized displaced oscillator basis of $N_b = 6$ (lines) or $N_b = 10$ (symbols) states per bin. Reprinted figures with permission from R. Bulla, H.-J. Lee, N.H. Tong, and M. Vojta, *Phys. Rev. B* **71**, 045122 (2005). Copyright 2005 by the American Physical Society.

grows with both N and α . The implication is that the chain NRG cannot access the asymptotic low-energy physics in the localized phase of the sub-ohmic spin-boson model. No such problem affects the localized phase of the ohmic case $s = 1$, or super-ohmic ($s > 1$) baths where the ground state is delocalized for any $\Delta \neq 0$.

Figure 6b illustrates results obtained using the star NRG. Since the oscillator shift θ_N is known analytically only for $\Delta = 0$, these calculations used a basis of N_b orthogonalized oscillator states chosen by minimizing the ground-state energy over multiple trial values of θ_N [27]. The figure demonstrates (for $s = 0.8$) that in both phases and on the phase boundary, $\langle b_N^\dagger b_N \rangle$ shows negligible difference for $N_b = 6$ and $N_b = 10$ and that the optimized basis seems to provide robust values for the boson occupancies, even in the localized phase where $\langle b_N^\dagger b_N \rangle$ is diverging. Despite this promising behavior, the star NRG proves to be unreliable in the delocalized phase and on the phase boundary, where its results are inconsistent with those obtained by other methods including chain NRG [27]. The reasons for this failure are not fully understood.

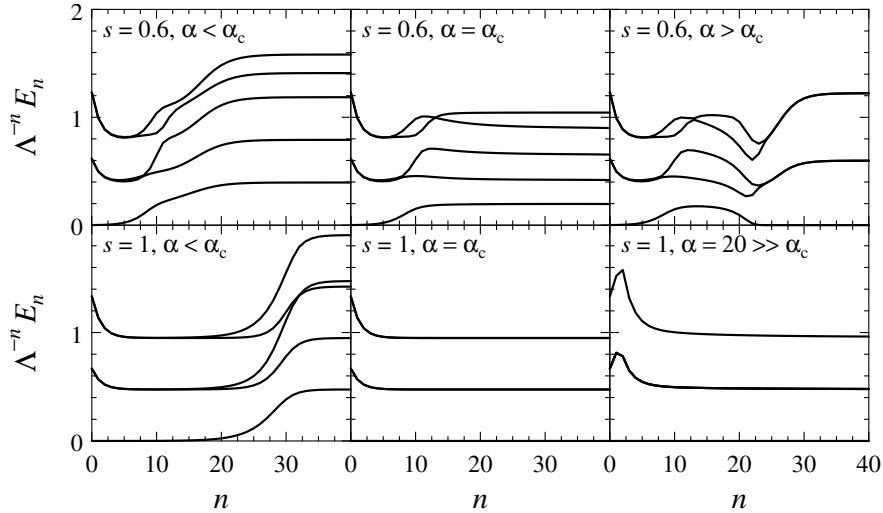


Fig. 7: NRG energies E_N vs. iteration number N for low-lying many-body eigenstates in the spin-boson model with $s = 0.6$ (top panels) and $s = 1$ (bottom panels) at dissipation strengths $\alpha < \alpha_c$ (left), $\alpha = \alpha_c$ (middle), and $\alpha > \alpha_c$ (right). Reprinted figure with permission from R. Bulla, N.-H. Tong, and M. Vojta, *Phys. Rev. Lett.* **91**, 170601 (2003). Copyright 2003 by the American Physical Society.

The conclusion from [27] is that neither the star NRG nor the chain NRG can provide a fully reliable treatment of all cases. Although the star NRG has been preferred in a study of a related model with ohmic dissipation [28], studies of the sub-ohmic spin-boson model have focused overwhelmingly on the chain approach. The next subsection will highlight a few successes and failures of the method.

3.3.2 Chain NRG results for the spin-boson model

Figure 7 illustrates for $s = 0.6$ and for $s = 1$ one of the primary outputs of the bosonic NRG method: the evolution of the low-lying many-body spectrum with iteration number N . When combined with the matrix elements of appropriate operators between the many-body eigenstates, the spectrum can yield information on static and dynamic quantities of interest, such as the static magnetization and the dynamical susceptibility of the impurity spin. Dynamical properties are not discussed in these lecture notes for reasons of space. The left panels in Fig. 7 exemplify the delocalized phase, where a rapid initial change in the energies E_N over the first few iterations is followed by one or two intermediate plateaus before final approach to a delocalized fixed-point spectrum. This spectrum, which is identical for all values of Δ and $\alpha < \alpha_c(\Delta)$, is just that of free bosons described by H_{bath} given in Eq. (12), reflecting the renormalization of the dissipative coupling α to zero throughout the delocalized phase.

Upon fine tuning of α extremely close to its critical value, as shown in the center panels of Fig. 7, an intermediate plateau (quite well developed in the left panel for $s = 1$, but barely visible in the $s = 0.6$ example) stretches beyond $N = 40$. For $s < 1$, this plateau spectrum is entirely distinct from that at the delocalized fixed point but is the same for all combinations $\Delta \neq 0$, $\alpha = \alpha_c(\Delta)$; it characterizes a *critical fixed point* located at nonzero critical couplings

$\Delta = \Delta^*(s)$, $\alpha = \alpha^*(s)$. In the localized phase (upper right panel of Fig. 7), the spectrum should in principle converge to a free-boson spectrum for a set of displaced oscillators, leading to a set of energies identical to those at the delocalized fixed point. However, due to bosonic truncation effects, the chain NRG instead yields a different, artificial fixed-point spectrum.

For $s = 1$, by contrast, the quantum phase transition at $\alpha = \alpha_c(\Delta)$ is governed by a *critical end point* at $\Delta^* = 0$, $\alpha^* = 1$, which terminates a line of localized fixed points $\Delta^* = 0$, $\alpha^* \geq 1$ [5]. For points (Δ, α) not too deep into the localized phase, α^* is sufficiently small that the chain NRG can faithfully reproduce the appropriate displaced oscillator ground state and its excitations, so the many-body spectrum for $N \rightarrow \infty$ is the same for all values of α (see the lower panels of Fig. 7).

Most NRG studies of the sub-ohmic spin-boson model have focused on the critical properties, which are very hard to access using algebraic methods. A particular focus has been the evaluation of critical exponents such as β and δ entering the variations

$$\phi(\alpha > \alpha_c, T = h = 0) \propto (\alpha - \alpha_c)^\beta \quad \text{and} \quad \phi(\alpha = \alpha_c, T = 0) \propto |h|^{1/\delta} \quad (18)$$

of the order parameter $\phi = \lim_{h \rightarrow 0^+} \langle S_z \rangle$, the exponents γ and x entering the variations

$$\chi(\alpha < \alpha_c, T = h = 0) \propto (\alpha_c - \alpha)^{-\gamma} \quad \text{and} \quad \chi(\alpha = \alpha_c, h = 0) \propto T^{-x} \quad (19)$$

of the order-parameter susceptibility $\chi = \partial\phi/\partial h|_{h=0}$, and the correlation-length exponent ν characterizing the vanishing according to

$$T^* \propto |\alpha - \alpha_c|^\nu \quad (20)$$

of the energy scale (extracted from data such as those shown in Fig. 7) at which the many-body spectrum flows away from the critical spectrum to that of either the delocalized or the localized fixed point. The chain NRG allows all these exponents to be determined to an unprecedented degree of numerical precision [26, 29]. Although they vary with s , the exponents are found to obey to within estimated numerical errors the *scaling relations*

$$\delta = (1 + x)/(1 - x), \quad \beta = \gamma(1 - x)/(2x), \quad \text{and} \quad \nu = \gamma/x \quad (21)$$

expected [30] to hold at an interacting quantum critical point in a magnetic impurity model below its upper critical dimension.

For $\frac{1}{2} < s < 1$, the observed scaling of exponents is consistent with expectations based on a mapping (carried out within a path-integral formulation [23]) of the spin-boson model onto a classical model for a chain of Ising spins with a long-range ferromagnetic interaction that decays with separation d like $d^{-(1+s)}$. The Ising model has a phase transition that is interacting for cases corresponding to $\frac{1}{2} < s < 1$ [31, 32]. Within this range, the NRG is fully consistent with the mapped classical problem, and the values of the exponents it produces agree with analytical limiting results where they are available. There is every indication that the chain-form bosonic NRG is yielding correct results over this range of weakly sub-ohmic bath exponents.

In contrast, for more slowly decaying interactions, corresponding in the spin-boson model to $0 < s < \frac{1}{2}$, the quantum critical point of the classical Ising chain is noninteracting and is characterized by mean-field exponents corresponding to $\beta = x = \frac{1}{2}$, $\delta = 3$, $\gamma = 1$, and $\nu = 1/s$. Of these values, only ν is in agreement with the NRG results. This discrepancy has led to considerable debate about the validity of the quantum-to-classical mapping. However, a preponderance of the evidence now points to deficiencies of the bosonic chain NRG in the treatment of mean-field (noninteracting) critical points:

- It has been pointed out [33] that above the upper critical dimension, the order-parameter exponent β and the magnetic exponent δ are properties not just of the vicinity of the critical point (where the chain NRG seems to be valid) but of the full flow to the delocalized fixed point (where truncation errors are known to be inevitable [27]). Indeed, a solution of the sub-ohmic spin-boson Hamiltonian in its NRG chain form using a *variational matrix product state* method that selects an optimized bosonic basis for chain site has shown for $s = 0.2, 0.3$, and 0.4 that the exponents take their mean-field (classical) values [34]. This result strongly highlights the importance of basis selection in NRG treatments of problems involving bosonic baths.
- A second (seemingly independent) effect has been proposed [33, 35, 36] to account for the difference between the thermal critical exponent $x = s$ found within the NRG and the classical value $x = \frac{1}{2}$. The basic idea [35] is that since the NRG at iteration N , corresponding to temperature $T \simeq \omega_c \Lambda^{-N}$, neglects all oscillator weight at frequencies $\omega \lesssim T$, the distance $\alpha - \alpha_c$ from criticality acquires temperature-dependent corrections. As a result, χ^{-1} calculated at $\alpha = \alpha_c(T = 0)$ acquires a spurious term $\propto T^s$ that dominates the underlying mean-field $T^{1/2}$ term. An *ad hoc* procedure for correcting this problem has been proposed [35], but it leads to some apparent inconsistencies [37]. Whether or not there is a rigorous fix for the mass-flow problem remains an important open question.

4 Bose-Fermi NRG

4.1 The Bose-Fermi Kondo model

The Bose-Fermi Kondo impurity model with Ising-symmetric bosonic coupling is described by the Hamiltonian $H_{\text{BFK}} = H_K + H_B$, where H_B is as given in Eq. (8) and

$$H_K = \sum_{\mathbf{k}, \sigma} \varepsilon_{\mathbf{k}} c_{\mathbf{k}\sigma}^\dagger c_{\mathbf{k}\sigma} + \frac{J}{2N_k} \mathbf{S} \cdot \sum_{\mathbf{k}, \mathbf{k}', \sigma, \sigma'} c_{\mathbf{k}\sigma}^\dagger \boldsymbol{\sigma}_{\sigma\sigma'} c_{\mathbf{k}'\sigma'} \quad (22)$$

is the standard Kondo Hamiltonian for the antiferromagnetic exchange coupling (with strength J) between an impurity spin- $\frac{1}{2}$ degree of freedom and the on-site spin of a conduction band. For the hybridization function in Eq. (3), H_K is the effective Hamiltonian to which the Anderson impurity model [Eq. (1)] reduces in the limit $0 < \Delta \ll -\varepsilon_d, U + \varepsilon_d$ in which real fluctuations

of the impurity occupancy are frozen out, and only the impurity spin degree of freedom remains active.

In this section, the conduction band dispersion $\varepsilon_{\mathbf{k}}$ is assumed to give rise to a density of states (per unit cell per spin orientation)

$$\rho(\varepsilon) \equiv N_k^{-1} \sum_{\mathbf{k}} \delta(\varepsilon - \varepsilon_{\mathbf{k}}) = \rho_0 |\varepsilon/D|^r \Theta(D - |\varepsilon|). \quad (23)$$

The case $r = 0$ represents a standard metal, while $r > 0$ describes a pseudogapped or semimetallic host. The bosonic bath is again taken to have a spectral function of the form given in Eq. (9) with the conventional replacement $2\pi\alpha \rightarrow (K_0 g)^2$, where K_0 is a density of states and g an energy.

The metallic ($r = 0$) Bose-Fermi Kondo model was originally introduced in the context of an extended dynamical mean-field theory for the two-band extended Hubbard model [38]. It has received most attention in connection with heavy-fermion quantum criticality, arising as an effective impurity problem in an extended dynamical mean-field treatment of the Kondo lattice model [39, 40]; here, the bosonic bath in the impurity problem embodies the effects, at a given Kondo lattice site, of the fluctuating magnetic field generated (via the Ruderman-Kittel-Kasuya-Yosida interaction) by local moments at other lattice sites. The $r = 0$ Bose-Fermi Kondo model with $s = 1$ also describes certain mesoscopic qubit devices, where the bosonic bath represents gate-voltage fluctuations [41], and the model has been invoked with $s = \frac{1}{2}$ and $s = \frac{1}{3}$ within a dynamical large- N treatment of a single-electron transistor coupled to both the conduction electrons and spin waves of ferromagnetic leads [42].

Perturbative renormalization-group studies of the $r = 0$ Bose-Fermi Kondo model [43, 44] indicate that for $0 < s \leq 1$, the competition between the conduction band and the bosonic bath for control of the impurity spin gives rise to a continuous quantum phase transition at $g = g_c(J)$ between a Kondo phase (for $g < g_c$) and a localized phase (for $g > g_c$). Just as in the spin-boson model, the phases can be distinguished by an order parameter $\phi = \lim_{h \rightarrow 0^+} \langle S_z \rangle$, where h is a local field that enters the Hamiltonian through a term $-hS_z$ added to H_{BFK} . In the localized phase, the order parameter increases as $(g - g_c)^\beta$ [cf. Eq. (18)]. For $g < g_c$, $\phi = 0$ but the effective Kondo temperature [the crossover scale to the low-temperature Fermi-liquid regime] vanishes continuously as $T_K \propto (g_c - g)^\nu$ [cf. Eq. (20)] describing a critical destruction of the Kondo many-body state. It is worth pointing out that although H_K exhibits SU(2) spin symmetry, the impurity-boson coupling lowers the overall symmetry of H_{BFK} to a U(1) invariance associated with conservation of the z component of local spin. This means that within any renormalization-group treatment, the Kondo exchange coupling evolves from $J\mathbf{S} \cdot \mathbf{s}_c$ (where \mathbf{s}_c is the conduction-band spin at the impurity site) to an effective form $J_z S_z s_{c,z} + \frac{1}{2} J_\perp (S^+ s_c^- + S^- s_c^+)$. It is the spin-flip coupling J_\perp that necessarily scales to infinity in the Kondo phase and to zero in the localized phase.

The fermionic pseudogap Kondo model described by Eqs. (22) and (23) with $r > 0$ has served as a paradigm for impurity quantum phase transitions [30, 45–47]. The suppression of the density of conduction states near the Fermi energy gives rise for $0 < r < \frac{1}{2}$ to a transition between

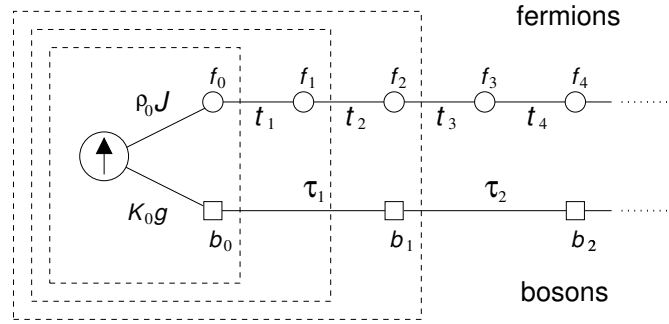


Fig. 8: Schematic representation of the Bose-Fermi NRG procedure for situations where the conduction half bandwidth D and the bosonic cutoff ω_c are of similar magnitudes. Since the bosonic tight-binding coefficients τ_n (and ξ_n , not shown) vary as Λ^{-n} , decaying twice as fast as the fermionic coefficients $t_n \propto \Lambda^{-n/2}$, the bosonic chain is extended by one site only at every other iteration. Dashed boxes from innermost to outermost enclose the degrees of freedom treated at NRG iterations $N = 0, 1$, and 2 . Adapted from [50].

an unscreened or local-moment phase for $J < J_c$ (where $\rho_0 J_c \simeq r$ for $r \ll \frac{1}{2}$) and a phase exhibiting partial Kondo screening of the impurity spin for $J > J_c$. The critical coupling J_c diverges as r approaches $\frac{1}{2}$ from below, and for $r \geq \frac{1}{2}$ the system is always in the local-moment phase where the impurity has a spin-doublet ground state. The pseudogap variant of the Bose-Fermi Kondo model has been proposed as a setting to explore the interplay between fermion- and boson-induced critical destruction of the Kondo effect [48].

4.2 NRG solution method

The Bose-Fermi Kondo model can be treated by suitably combining [49, 50] elements of the NRG treatment of pure-fermionic models (as summarized at the start of Sec. 2.2) and the NRG formulation of pure-bosonic models (as described in Sec. 3.2). Since the conduction band part of the Hamiltonian is mapped onto the tight-binding form in Eq. (5), it is convenient also to treat the bosonic bath part in the chain representation [Eq. (12)] rather than the alternative star formulation. The NRG iteration scheme must take into account that the fermionic hopping coefficients are proportional to $\Lambda^{-n/2}$ whereas the bosonic tight-binding coefficient decay as Λ^{-n} . It is in the spirit of the NRG for each iteration to treat fermions and bosons of the same energy scale. This can be achieved by adding one site to the fermionic chain at each iteration but extending the bosonic chain only at every other iteration. In situations where D and ω_c are not too different in magnitude, one can adopt the scheme shown schematically in Fig. 8 where bosonic site n is introduced at iteration $N = 2n$. (If $\omega_c \ll D$, it is more appropriate to delay the incorporation of bosonic site 1 until some iteration $N = M > 2$, and then to introduce bosonic sites $n > 1$ at iteration $N = M + 2n - 2$.)

To date, all NRG calculations for Bose-Fermi models such as H_{BFK} have been performed using a bosonic basis of eigenstates of $b_n^\dagger b_n$ with eigenvalues n_b satisfying $0 < n_b < N_b$. If one retains N_s many-body eigenstates after each iteration, then the CPU time is proportional to $(4N_b N_s)^3$ at any iteration where the bosonic chain is extended, and is otherwise proportional to $(4N_s)^3$.

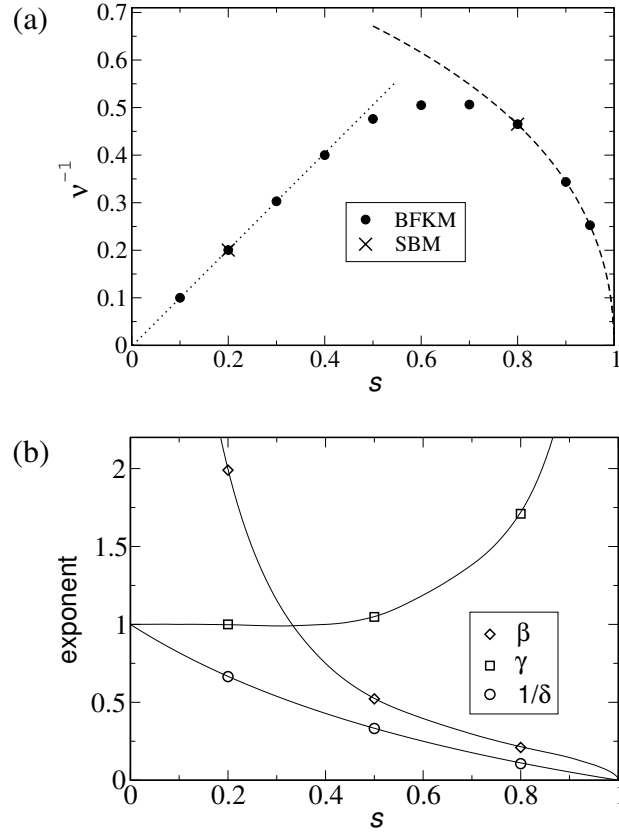


Fig. 9: Critical exponents of the Bose-Fermi Kondo model vs. bath exponent s : (a) Reciprocal correlation length exponent ν^{-1} , comparing NRG results for the Bose-Fermi Kondo model (circles) with those for the spin-boson model (crosses). The dotted line plots the mean-field dependence $\nu^{-1} = s$, while the dashed line shows the form $\nu^{-1} = \sqrt{2(1-s)} + C$ with $C = O(1)$ that arises in a perturbative expansion about $s = 1$. (b) Exponents β , γ , and $1/\delta$. Symbols show values directly computed within the NRG, while the lines come from substituting NRG values for $\nu(s)$ and $x(s)$ into the scaling relations in Eqs. (21). Reprinted from [50].

The additional factor of 4^3 at iterations of the former type compared to the iteration time in pure-bosonic problems such as the spin-boson model makes the NRG treatment of H_{BFK} quite computationally intensive. In comparison with a standard Kondo or Anderson problem, the computational time grows by a factor even greater than N_b^3 because it is generally necessary to increase N_s for the Bose-Fermi problem to achieve similar levels of accuracy. For $N_b = 8$, the overall time increase may be of order 10^4 – 10^5 .

4.3 Results

4.3.1 Metallic band ($r = 0$)

The NRG scheme described in Sec. 4.2 has been used to carry out a detailed study of the Bose-Fermi Kondo model with Ising-symmetric bosonic coupling [49, 50]. The principal finding of this work is that for sub-ohmic exponents $0 < s < 1$, the quantum critical point of the model is described by s -dependent critical exponents that are identical within numerical error to those

for the spin-boson model with the same bath exponent. This conclusion is illustrated in Fig. 9a, which compares Bose-Fermi Kondo and spin-boson values for the correlation-length exponent ν [defined in Eq. (20)]. Figure 9b compares directly computed values of β , γ , and δ [see Eqs. (18) and (19)] with ones derived from NRG values for $\nu(s)$ and $x(s)$ using the scaling relations in Eqs. (21). The NRG gives $x = s$ across the entire range $0 < s < 1$.

Given the lessons learned from the spin-boson model (see Sec. 3.3), it seems quite possible that the finding of an interacting critical point in the Bose-Fermi Kondo model for $0 < s < \frac{1}{2}$ is an artifact of the NRG treatment of the bosonic bath. This is not absolutely certain because there is a symmetry difference between the two problems. The Bose-Fermi Kondo model has $U(1)$ spin-rotational invariance about the z axis plus an additional Z_2 symmetry for longitudinal field $h = 0$. There are no such symmetries in the spin-boson model due to the nonzero value of Δ that must be present to induce a quantum phase transition. A recent study of a two-bath generalization of the spin-boson model in which the baths couple to different components of the impurity spin has found that a quantum critical point is classical in the presence of a transverse field but non-classical in the absence of the field where an additional Z_2 symmetry exists [34, 51]. Whether such a difference exists between the Bose-Fermi Kondo and one-bath spin-boson models is an interesting question.

4.3.2 Pseudogapped band ($r > 0$)

This subsection is devoted to the pseudogap variant of the Bose-Fermi Kondo model described by a density of states of the form of Eq. (23) with $0 < r < \frac{1}{2}$ and a bosonic bath exponent $\frac{1}{2} < s < 1$. For $g = 0$, the bosons decouple from the rest of the system and for $r > 0$ the model exhibits fermion-driven critical destruction of the Kondo effect at some $J = J_c(r, g = 0)$ [30, 45–47]. For $r = 0$, as described in the preceding paragraphs, the model instead features boson-driven Kondo destruction. This raises the question of the nature of the quantum critical point or points in situations where the fermionic and bosonic Kondo-destruction mechanisms are both present. The issue has been elucidated in [48], which presents NRG solutions of H_{BFK} for numerous combinations of exponents (r, s) , corroborated by continuous-time quantum Monte Carlo treatments of the corresponding Bose-Fermi Anderson model ($H_{\text{BFA}} = H_A + H_B$) for $(r, s) = (0.4, 0.6)$ and $(0.4, 0.8)$. In all cases $g > 0$, a continuous quantum phase transition occurs at some $J = J_c(r, s, g)$ between Kondo ($J > J_c$) and localized ($J < J_c$) phases. The physics in the former phase is essentially that of the Kondo-screened phase of the pseudogap Kondo model, modified by an irrelevant coupling to the bosons, while the localized phase behaves like that of the spin-boson model with irrelevant corrections from the Kondo coupling.

While continuous quantum phase transitions between phases in which the impurity degree of freedom is respectively quenched and asymptotically free are found in a number of models, including several discussed above, an interesting new feature of the pseudogap Bose-Fermi Kondo model is the existence of three qualitatively different types of quantum criticality, each accessed within a different region of the (r, s) space, as shown in Fig. 10:

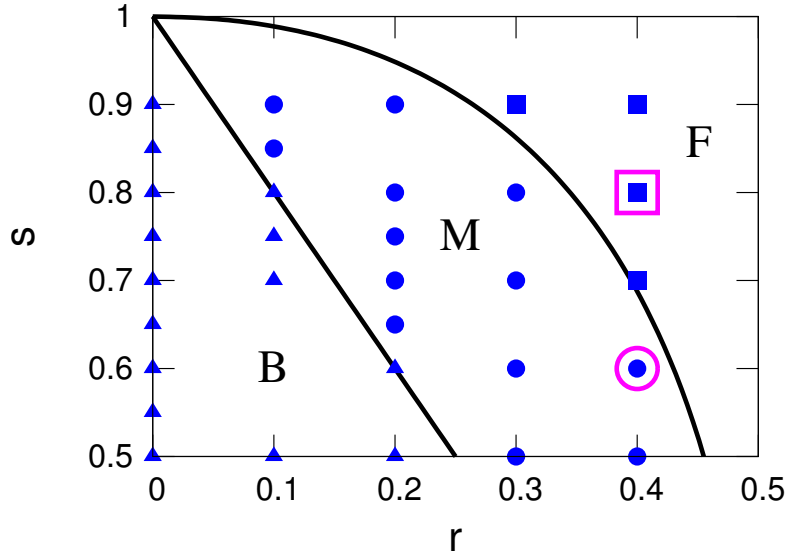


Fig. 10: Summary of the quantum criticality found in the pseudogap Bose-Fermi Kondo model for different band exponents r and bath exponents s . Squares, triangles, and circles respectively denote quantum criticality of the F, B, and M types described in the text. Filled symbols represent NRG results for the Bose-Fermi Kondo model while open symbols represent continuous-time quantum Monte Carlo results for the Bose-Fermi Anderson model. Solid lines show the conjectured boundaries $s = 1 - 2r$ and $x_B(s) = s = x_F(r)$ between the different types of criticality. Reprinted from [48].

- *Fermionic- or F-type criticality* arises in cases where the critical spin fluctuations induced by the band pseudogap are more divergent for temperatures $T \rightarrow 0$ than those resulting from the bosonic coupling. Specifically, F-type criticality occurs for all (r, s) such that the thermal critical exponent $x_F(r)$ of the pseudogap Kondo model—which is given by $x_F \simeq 1 - (\rho_0 J_c)^2$ for $0 < r \ll \frac{1}{2}$ [30] but in general must be determined numerically—is smaller than that of the spin-boson model $x_B(s) = s$ [see Eq. (19)]. The asymptotic low-energy spectrum calculated within the NRG recovers the $SU(2)$ spin symmetry broken by the bosonic coupling g , and this spectrum decomposes into a direct product of the spectrum of free bosons with bath exponent s [that of H_b in Eq. (12)] and the critical spectrum of the pseudogap Kondo model with band exponent r , i.e., (BF critical) = (B free) \otimes (F critical). All calculated critical exponents are identical to those of the pure-fermionic pseudogap Kondo model with the same r .
- *Bosonic- or B-type criticality* is fully governed by the bosonic bath, a condition that (for reasons that have yet to be fully understood) occurs for $s < 1 - 2r$. The fixed-point spectrum exhibits $SU(2)$ spin symmetry and decomposes into a direct product of the critical spectrum of the spin-boson model with bath exponent s and the Kondo-phase spectrum of the pseudogap Kondo model with band exponent r , i.e., (BF critical) = (B critical) \otimes (F Kondo). All calculated critical exponents are identical to those of the metallic ($r = 0$) Bose-Fermi Kondo model with the same s .

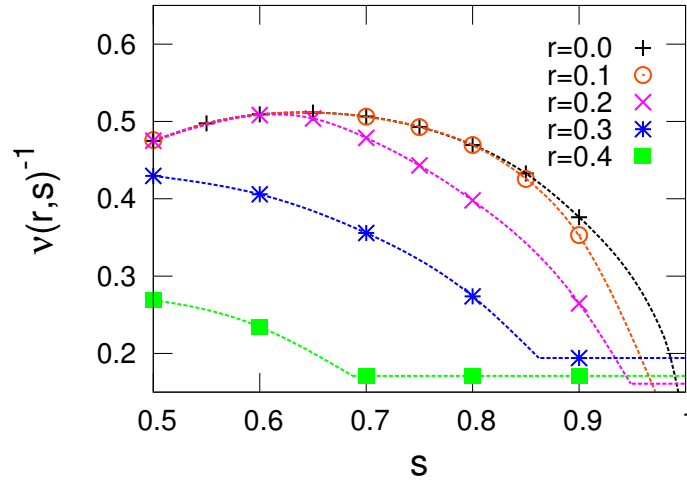


Fig. 11: Reciprocal of the Bose-Fermi Kondo model correlation length exponent $1/\nu$ vs. bath exponent s for the metallic case $r = 0$ and for pseudogaps described by $r = 0.1-0.4$. The $r = 0$ exponents coincide with those of the corresponding spin-boson model and represent the values $1/\nu_B(s)$ describing pure-bosonic criticality. Each horizontal line segment shows a pure-fermionic value $1/\nu_F(r)$. The Bose-Fermi Kondo exponent coincides with $1/\nu_B(s)$ for $s < 1 - 2r$ and with $1/\nu_F(r)$ for $s \geq x_F(r)$. For $1 - 2r < s < x_F(r)$, $1/\nu(r, s)$ lies in between the bosonic and fermionic values. Reprinted from [48].

- *Mixed- or M-type criticality* is found across the range of intermediate s values such that $1 - 2r < s < x_F(r)$. The fixed-point spectrum exhibits broken $SU(2)$ spin symmetry and does not decompose into a direct product of bosonic and fermionic parts. The thermal exponent x takes its spin-boson model value $x_B(s) = s$ but the correlation-length exponent lies between the values for the spin-boson model and the pseudogap Kondo model, i.e., $\nu_F^{-1}(r) < \nu^{-1}(r, s) < \nu_B^{-1}(s)$, as illustrated in Fig. 11. Just as for the F- and B-types, all other calculated exponents obey the scaling relations in Eqs. (21), indicating that the quantum critical point is interacting.

It is important to consider whether the NRG accurately captures the quantum phase transitions of the pseudogap Bose-Fermi Kondo model. Given that over the entire region $0 < r < \frac{1}{2}$, $\frac{1}{2} < s < 1$ the exponent x determined using the NRG is *larger* than its mean-field counterpart $x = \frac{1}{2}$, it does not seem possible that the true critical behavior is being masked by the mass-flow problem identified in the spin-boson model for $0 < s < \frac{1}{2}$. Since the exponent ν can be determined entirely in the Kondo phase, it should be immune to the truncation errors that plague the localized phase (an immunity that has been found to be present in the spin-boson model [29]). These observations provide strong grounds for believing that the Bose-Fermi NRG method correctly accounts for the quantum critical behavior over the range of bath exponents considered.

Mixed quantum criticality arising from a nontrivial interplay between fermionic and bosonic critical fluctuations constitutes a new universality class of impurity quantum phase transitions distinct from those of the pseudogap Kondo model and the spin-boson model. This intriguing finding provides a motivation to search for yet other universality classes in models that may be more readily realized than the pseudogap Bose-Fermi Kondo model.

5 Closing

The goal of these lectures notes has been to introduce the main technical issues surrounding the extension of the NRG method to treat quantum impurity models that include bosonic degrees of freedom, to lay out the steps that have been developed to addresses these issues, and to provide an idea of the capabilities and limitations of the method that results. Space limitations have precluded description of the calculation of Green's functions and correlation functions, details of which can be found in some of the references, and have forced omission of many interesting applications as well as discussion of topical issues such as the treatment of systems out of equilibrium.

Acknowledgments

I acknowledge support from the National Science Foundation Materials World Network program under Grant No. DMR-1107814.

References

- [1] K.G. Wilson, *Rev. Mod. Phys.* **47**, 773 (1975)
- [2] H.R. Krishna-murthy, J.W. Wilkins, and K.G. Wilson, *Phys. Rev. B* **21**, 1003 (1980); *ibid.* **21**, 1044 (1980)
- [3] R. Bulla, T.A. Costi, and Th. Pruscke, *Rev. Mod. Phys.* **80**, 395 (2008)
- [4] T. Costi: *NRG and Multiorbital Kondo Physics* in: E. Pavarini, E. Koch, and P. Coleman (eds.): *Many-Body Physics: From Kondo to Hubbard*, Modeling and Simulation, Vol. 5 (Forschungszentrum Jülich, 2015)
<http://www.cond-mat.de/events/correl15>
- [5] A.J. Leggett, S. Chakravarty, A.T. Dorsey, M.P.A. Fisher, A. Garg, and W. Zwerger, *Rev. Mod. Phys.* **59**, 1 (1987)
- [6] U. Weiss: *Quantum Dissipative Systems* (4th ed., World Scientific, Singapore, 2012)
- [7] F.D.M. Haldane, *Phys. Rev. B* **15**, 2477 (1977)
- [8] K. Schönhammer and O. Gunnarsson, *Phys. Rev. B* **30**, 3141 (1984)
- [9] A.C. Hewson and D. Meyer, *J. Phys.: Condens. Matter* **14**, 427 (2002)
- [10] H.C. Lee and H.-Y. Choi, *Phys. Rev. B* **69**, 075109 (2004)
- [11] E. Šimánek, *Solid State Commun.* **32**, 731 (1979)
- [12] C.S. Ting, D.N. Talwar, and K.L. Ngai, *Phys. Rev. Lett.* **45**, 1213 (1980)
- [13] H.-B. Schüttler, and A.J. Fedro, *Phys. Rev. B* **38**, 9063 (1988)
- [14] P.S. Cornaglia, H. Ness, and D.R. Grempel, *Phys. Rev. Lett.* **93**, 147201 (2004)
- [15] P.S. Cornaglia, D.R. Grempel, and H. Ness, *Phys. Rev. B* **71**, 075320 (2005)
- [16] J. Paaske and K. Flensberg, *Phys. Rev. Lett.* **95**, 176801 (2005)
- [17] For compactness of notation, we drop all factors of the reduced Planck constant \hbar , Boltzmann's constant k_B , the impurity magnetic moment $g\mu_B$, and the electronic charge e , as well as the zero-point energy of every harmonic oscillator.
- [18] P.W. Anderson, *Phys. Rev.* **124**, 41 (1961)
- [19] M. Cheng, M.T. Glossop, and K. Ingersent, *Phys. Rev. B* **80**, 165113 (2009)
- [20] C. Lanczos, *J. Res. Natl. Bur. Stand.* **45**, 255 (1950)
- [21] G. Iche and A. Zawadowski, *Solid State Commun.* **10**, 1001 (1972)

- [22] A. Taraphder and P. Coleman Phys. Rev. Lett. **66**, 2814 (1991)
- [23] H. Spohn and R. Dümcke, J. Stat. Phys. **41**, 389 (1985)
- [24] F. Guinea, V. Hakim, and A. Muramatsu, Phys. Rev. B **32**, 4410 (1985)
- [25] T.A. Costi and C. Kieffer, Phys. Rev. Lett. **76**, 1683 (1996)
- [26] R. Bulla, N.-H. Tong, and M. Vojta, Phys. Rev. Lett. **91**, 170601 (2003)
- [27] R. Bulla, H.-J. Lee, N.H. Tong, and M. Vojta, Phys. Rev. B **71**, 045122 (2005)
- [28] J. Sabio, L. Borda, F. Guinea, and F. Sols, Phys. Rev. B **78**, 085439 (2008)
- [29] M. Vojta, N.-H. Tong, and R. Bulla, Phys. Rev. Lett. **94**, 070604 (2005)
- [30] K. Ingersent and Q. Si, Phys. Rev. Lett. **89**, 076403 (2002)
- [31] M.E. Fisher, S. Ma, and B.G. Nickel, Phys. Rev. Lett. **29**, 917 (1972)
- [32] E. Luijten and H.W.J. Blöte, Phys. Rev. B **56**, 8945 (1997)
- [33] M. Vojta, N.-H. Tong, and R. Bulla, Phys. Rev. Lett. **102**, 249904(E) (2009)
- [34] C. Guo, A. Weichselbaum, J. von Delft, and M. Vojta, Phys. Rev. Lett. **108**, 160401 (2012)
- [35] M. Vojta, R. Bulla, F. Güttge, and F. Anders, Phys. Rev. B **81**, 075122 (2010)
- [36] M. Vojta, Phys. Rev. B **85**, 115113 (2012)
- [37] S. Kirchner, K. Ingersent, and Q. Si, Phys. Rev. B **85**, 075113 (2012)
- [38] J.L. Smith and Q. Si, Europhys. Lett. **45**, 228 (1999)
- [39] Q. Si, S. Rabello, K. Ingersent, and J.L. Smith, Nature (London) **413**, 804 (2001)
- [40] Q. Si, S. Rabello, K. Ingersent, and J.L. Smith, Phys. Rev. B **68**, 115103 (2003)
- [41] K. Le Hur, Phys. Rev. Lett. **92** 196804 (2004)
- [42] S. Kirchner, L. Zhu, Q. Si, and D. Natelson, Proc. Natl. Acad. USA **102**, 18824 (2005)
- [43] L. Zhu and Q. Si, Phys. Rev. B **66**, 024426 (2002)
- [44] G. Zaránd and E. Demler, Phys. Rev. B **66**, 024427 (2002)
- [45] D. Withoff and E. Fradkin, Phys. Rev. Lett. **64**, 1835 (1990)
- [46] C. Gonzalez-Buxton and K. Ingersent, Phys. Rev. B **57**, 14254 (1998)
- [47] L. Fritz and M. Vojta, Phys. Rev. B **70** 214427 (2004)

-
- [48] J. Pixley, S. Kirchner, K. Ingersent, and Q. Si, *Phys. Rev. B* **88**, 245111 (2013)
- [49] M.T. Glossop and K. Ingersent, *Phys. Rev. Lett.* **95**, 067202 (2005)
- [50] M.T. Glossop and K. Ingersent, *Phys. Rev. B* **75**, 104410 (2007)
- [51] B. Bruognolo, A. Weichselbaum, C. Guo, J. von Delft, I. Schneider, and M. Vojta, *Phys. Rev. B* **90**, 245130 (2014)